Molecular and Cellular Endocrinology 419 (2016) 172–184

Contents lists available at ScienceDirect

Molecular and Cellular Endocrinology

journal homepage: www.elsevier.com/locate/mce

Compound heterozygous *DUOX2* gene mutations (c.2335-1G>C/c.3264_3267delCAGC) associated with congenital hypothyroidism. Characterization of complex cryptic splice sites by minigene analysis

Fiorella S. Belforte [a, c], Cintia E. Citterio [b, c], Graciela Testa [d], María Cecilia Olcese [a, c], Gabriela Sobrero [d], Mirta B. Miras [d], Héctor M. Targovnik [b, c], Carina M. Rivolta [a, c, *]

[a] *Laboratorio de Genética Molecular Tiroidea, Instituto de Inmunología, Genética y Metabolismo (INIGEM, CONICET-UBA), Hospital de Clínicas "José de San Martín", C1120AAR Buenos Aires, Argentina*
[b] *Laboratorio de Genética y Biología Molecular, Instituto de Inmunología, Genética y Metabolismo (INIGEM, CONICET-UBA), Hospital de Clínicas "José de San Martín", C1120AAR Buenos Aires, Argentina*
[c] *Cátedra de Genética (FFyB-UBA), C1113AAD Buenos Aires, Argentina*
[d] *Servicio de Endocrinología, Hospital de Niños Santísima Trinidad, 5000 Córdoba, Argentina*

ARTICLE INFO

Article history:
Received 19 July 2015
Received in revised form
25 September 2015
Accepted 19 October 2015
Available online 24 October 2015

Keywords:
Congenital hypothyroidism
DUOX2 gene
Mutation
Compound heterozygous mutations
Cryptic splice site

ABSTRACT

Iodide Organification defects (IOD) represent 10% of cases of congenital hypothyroidism (CH) being the main genes affected that of *TPO* (thyroid peroxidase) and *DUOX2* (dual oxidasa 2). From a patient with clinical and biochemical criteria suggestive with CH associated with IOD, *TPO* and *DUOX2* genes were analyzed by means of PCR-Single Strand Conformation Polymorphism analysis and sequencing. A novel heterozygous compound to the mutations c.2335-1G>C (paternal mutation, intron 17) and c.3264_3267delCAGC (maternal mutation, exon 24) was identified in the *DUOX2* gene. Ex-vivo splicing assays and subsequent RT-PCR and sequencing analyses were performed on mRNA isolated from the HeLa cells transfected with wild-type and mutant pSPL3 expression vectors. The wild-type and c.2335-1G>C mutant alleles result in the complete inclusion or exclusion of exon 18, or in the activation of an exonic cryptic 5′ ss with the consequent deletion of 169 bp at the end of this exon. However, we observed only a band of the expected size in normal thyroid tissue by RT-PCR. Additionally, the c.2335-1G>C mutation activates an unusual cryptic donor splice site in intron 17, located at position −14 of the authentic intron 17/exon 18 junction site, with an insertion of the last 14 nucleotides of the intron 17 in mutant transcripts with complete and partial inclusion of exon 18. The theoretical consequences of splice site mutation, predicted with the bioinformatics NNSplice, Fsplice, SPL, SPLM and MaxEntScan programs were investigated and evaluated in relation with the experimental evidence. These analyses confirm that c.2335-1G>C mutant allele would result in the abolition of the authentic splice acceptor site. The results suggest the coexistence in our patient of four putative truncated proteins of 786, 805, 806 and 1105 amino acids, with conservation of peroxidase-like domain and loss of gp91^{phox}/NOX2-like domain. In conclusion a novel heterozygous compound was identified being responsible of IOD. Cryptic splicing sites have been characterized in *DUOX2* gene for the first time. The use of molecular biology techniques is a valuable tool for understanding the molecular pathophysiology of this type of thyroid defects.

1. Introduction

Thyroid dyshormonogenesis is a defect in thyroid hormone biosynthesis, which accounts for the 15–20% of the primary Congenital Hypothyroidism (CH) cases (Cavarzere et al., 2008). Patients with dyshormonogenesis have a broad spectrum of disease phenotypes, with or without brain involvement. These endocrine disorders has been linked to mutations in the *SLC5A5* (solute carrier

* Corresponding author. Laboratorio de Genética Molecular Tiroidea, Instituto de Inmunología, Genética y Metabolismo (INIGEM, CONICET-UBA), Hospital de Clínicas "José de San Martín", Av. Córdoba 2351, Cuarto Piso, Sala 5, C1120AAR, Buenos Aires, Argentina.
E-mail addresses: cmrivolta@conicet.gov.ar, crivolta@ffyb.uba.ar (C.M. Rivolta).

http://dx.doi.org/10.1016/j.mce.2015.10.014
0303-7207/

family 5 member 5, *NIS*) (Spitzweg and Morris, 2010], *SLC26A4* (solute carrier family 26 member 4, *pendrin*) (Bizhanova and Kopp, 2010), *TPO* (thyroid peroxidase) (Ris-Stalpers and Bikker, 2010), *DUOX2* (dual oxidasa 2) (Grasberger, 2010), *DUOXA2* (DUOX maturation factor 2) (Grasberger et al., 2012; Hulur et al., 2011; Liu et al., 2015; Yi et al., 2013; Zamproni et al., 2008), *IYD* (iodotyrosine deiodinase, *DEHAL1*) (Moreno and Visser, 2010) and *TG* (thyroglobulin) (Targovnik et al., 2010, 2011) genes. Dyshormonogenesis results frequently in a bilobed cervical goiter due to trophic action of the elevated TSH level (Grasberger and Refetoff, 2011; Targovnik et al., 2011). Iodide organification defects (IOD) are associated with mutations in the *TPO*, *DUOX2*, *DUOXA2* or *SLC26A4* genes and characterized by a positive perchlorate descarge test (PDT) (Fugazzola et al., 2011; Grasberger and Refetoff, 2011).

DUOX2 is a member of the NOX/DUOX family, which is expressed at the apical membrane of thyroid follicular cells. DUOX2 produces hydrogen peroxide (H_2O_2) which is required for the iodination and coupling of hormonogenic tyrosyl residues of TG (De Deken et al., 2000; Dupuy et al., 1999; Ohye and Sugawara, 2010). The *DUOX2* gene (GenBank accession number NT_010194) is located on chromosome 15q15.3 spanning 22 Kb of genomic DNA which includes 34 exons, being the first non-coding. The mRNA (GenBank accession number NM_014080) is 6376 nucleotide long and the preprotein is composed of a putative 25 amino acids signal peptide followed by a 1523 amino acids polypeptide encoding a peroxidase homology ectodomain (peroxidase-like domain) and a $gp91^{phox}$/NOX2-like domain (De Deken et al., 2000; Dupuy et al., 1999; Morand et al., 2004; Ohye and Sugawara, 2010). A truncated *DUOX2* splicing variant has been identified in the rat thyroid cell line FRTL5 (Morand et al., 2003). However, little is known about the alternative splicing mechanism of *DUOX2* gene.

Monoallelic *DUOX2* mutations (dominant inheritance) have been found in transient to mild permanent CH, whereas biallelic mutations (recessive inheritance) have been associated with transient to severe permanent CH (Fugazzola et al., 2011; Grasberger, 2010). Up to date, sixty-eight mutations in the human *DUOX2* gene have been identified and characterized: 3 splice site (ss) mutations, 8 nonsense mutations, 43 missense mutations and 14 deletions and insertions (Abe et al., 2015; Cangul et al., 2014; Chai et al., 2015; De Marco et al., 2011, Di Candia et al., 2006; Grasberger et al., 2007; Hoste et al., 2010; Hulur et al., 2011; Jin et al., 2014, Kasahara et al., 2013; Lü et al., 2011; Maruo et al., 2008; Moreno et al., 2002; Muzza et al., 2014; Narumi et al., 2011; Ohye et al., 2008; Pfarr et al., 2006; Satoh et al., 2015; Schoenmakers et al., 2013; Tonacchera et al., 2009; Varela et al., 2006; Vigone et al., 2005; Wang et al., 2014; Yoshizawa-Ogasawara et al., 2013).

In the present study we report a patient with CH and high levels of serum TG. Analysis of *DUOX2* gene revealed a previously documented c.2335-1G>C (g.IVS17-1G>C)) mutation (Muzza et al., 2014) and a novel c.3264_3267delCAGC mutation, conforming a new compound heterozygous. Acceptor ss mutation in intron 17 results in complete inclusion or exclusion of exon 18, or in the activation of an exonic cryptic 5′ ss with partial inclusion of exon 18. Remarkable, in addition of complete or partial inclusion of exon 18 in the c.2335-1G>C mutation form, the insertion of the last 14 nucleotides of the intron 17 was originate by activation of an unusual intronic cryptic 3′ ss. The competition between an activated cryptic ss and the authentic ss, as can be seen in the present report, represents an interesting field for the study of ss characteristics.

2. Materials and methods

2.1. Patient

We report a boy born in 2006 affected with CH and the first child of healthy, non-consanguineous parents. He was born at term with appropriate weight for gestational age, normal delivery. Apgar score was 7/8 at 1 and 5 min. The clinical examination was normal and he did not show goiter. He was diagnosed by newborn screening on day 6 of life, being neonatal TSH of 33 mIU/L (Cut off: 10 mIU/L). The hypothyroidism diagnosis was confirmed at 11 days of age with TSH: 62 mIU/L (reference range: 0.8–8.9), Total T4: 4.92 μg/dl (reference range: 7.4–19.1), Free T4: 0.6 ng/dl (reference range 1.2–2.8), Total T3: 139 ng/dl (reference range: 137–321) and TG: 874 ng/ml (reference range:11–200) with no circulating autoantibodies (anti-TPO and anti-TG). Thyroid ultrasound showed a gland of normal location, size and morphology. Thyroid volume was calculated by multiplication of length, breadth and depth and a corrective factor of 0.52 for each lobe. Volume of the right lobe: 0.37 ml (reference range: 0.3–1.4) and volume of the left lobe: 0.39 ml (reference range: 0.4–1.7). The ^{99}Tc scintigraphy confirmed a normally located gland with normal radiotracer uptake. Bone age: both ossification centers were present in knee X-rays. Echocardiogram was normal. The patient started the treatment with Levothyroxine at the age of 11 days at a dose of 11 μg/Kg/day. At one month of life the first clinical and laboratory control under treatment were normal; TSH: 0.4 mIU/L (reference range: 0.85–7.79) Free T4: 1.88 ng/dl (reference range: 1.01–2.09). Compliance to Levothyroxine treatment was adequate and he remains euthyroid. He shows adequate growth and development. At this moment, he attends primary school without learning difficulties.

Written informed consent to participate in the clinical and genetic studies was given by both parents and the research project was approved by the Institutional Review Board.

2.2. PCR amplification

Genomic DNA was isolated from peripheral blood leucocytes by the standard cetyltrimetilammonium bromide (CTAB) method and stored at −20 °C up to the analysis.

The promotor region and all 17 exons of the human *TPO* gene including splicing signals and the flanking regions of each intron, and the complete coding sequence of the human *DUOX2* gene, along with the flanking regions of each intron were amplified using the primers and PCR conditions reported previously (Rivolta et al., 2003; Varela et al., 2006). The amplified products were analyzed in 2% agarose gel.

2.3. Single Strand Conformation Polymorphism (SSCP) analysis

SSCP analysis was used to screen for the presence of mutations in each exon of the *TPO* and *DUOX2* genes and their flanking intronic regions. The gel matrix for SSCP contained 8%, 10% or 12% polyacrylamide (29:1), with or without 10% glycerol. Samples were electrophoresed for 17–43 h at a constant temperature (4 °C). DNA was visualized by silver staining.

2.4. DNA sequencing

TPO and *DUOX2* PCR products showing an aberrant pattern in SSCP analysis were purified by GFX PCR DNA and Gel Band Purification Kit (GE Healthcare, Little Chalfont, Buckinghamshire, UK) and directly sequenced using sense- and antisense-specific primers reported previously with the Big Dyedeoxyterminator Cycle Sequencing Kit (Applied Biosystems, Weiterstadt, Germany). The samples were analyzed on the 3130xl and 3500xl Genetic Analyzer (Applied Biosystems).

Sequence variants are numbered according to *DUOX2* mRNA reference sequences reported in National Center for Biotechnology Information (NCBI), accession number: NM_014080.4. The 'A' of the

ATG start codon is denoted as nucleotide +1 being the initiator methionine, the codon 1. Splicing mutations are annotated by using cDNA sequences and old nomenclature (g.IVS) is included in parenthesis.

2.5. Cloning of wild-type and mutated exons 24 PCR fragments

The amplified fragment corresponding to exon 24 from index patient II-1 was T-A cloned into pGEM-T Easy vector (Promega, Madison, WI, USA). DNA sequencing was performed as described above from wild type and mutant allele clones using the intronic primers DUOX2-24F and DUOX2-24R (Varela et al., 2006).

2.6. Construction and expression of the minigenes

To study the effect of the c.2335-1G>C mutation, we constructed wild-type and mutated hybrid minigenes using the vector pSPL3 (Life Technologies Inc., Gaithersburg, MD). The genomic DNA region from index patient II-1 containing exon 18 (226-bp) and intronic flanking sequences (1228-bp upstream from the 5′ exon end and 65-bp downstream from the 3′ exon end) were amplified by long PCR technique using elongase (Invitrogen, Carsbad, CA). The forward primer (SPL3-I17-F), 5′-ATAAGAATGCGGCCGCGAAACCTGGGCTGCATAGAA-3′, contained the NotI site (underlined) and the reverse primer (SPL3-I18-R), 5′-CAGGATCCCAGGTCATCTCCTTGCTGAAA-3′, contained the BamHI site (underlined). The 1543-bp (1519 of which were intron 17/exon 18/intron 18 *DUOX2* sequences) PCR product was sequentially digested with NotI and BamHI. The insert was directionally cloned into the NotI and BamHI sites of the pSPL3 vector. Because index patient II-1 is heterozygous for the c.2335-1G>C mutation, the wild-type and mutated alleles were thus cloned. The recombinant plasmids were amplified in DH5α-competent cells and purified by use of the Wizard Plus SV Minipreps DNA Purification System (Promega). The correct sequence was confirmed by sequencing with DUOX2-18R intronic primers (Varela et al., 2006).

HeLa cells were grown in 3.8-cm dishes in DMEM supplemented with 10% fetal bovine serum and 100 U/ml penicillin-streptomycin (Invitrogen) in a 5% CO_2 atmosphere at 37 °C. When cells reached approximately 80% confluence, they were transfected with 500 ng of plasmid DNA (wild-type, mutant, and control pSPL3)/3.8-cm dish with the Lipofectamine 2000 (Invitrogen). Twenty four hours later, cells were harvested and total RNA was extracted with SV Total RNA Isolation System (Promega).

The RT-PCR was performed using vector-specific primers: forward primer (pSPL3F), 5′-TCTGAGTCACCTGGACAACC-3′ and reverse primer (pSPL3R), 5′- ATCTCAGTGGTATTTGTGAGC-3′. Samples were heated to 94 °C for 5 min, followed by 39 cycles of DNA denaturation (94 °C for 30 s), annealing (55 °C for 30 s), and polymerization (72 °C for 1 min). After the last cycle, the samples were incubated for additional 10 min at 72 °C. The RT-PCR products were purified from the agarose gel by using the Illustra GFX PCR DNA and Gel Band Purification Gel (GE Healthcare), cloned into pGEM-T Easy vector (Promega) and then sequenced with the pSPL3F and pSPL3R vector primers.

2.7. RT-PCR experiment

Total RNA was prepared from human thyroid tissue using TRIzol Reagent. cDNA was synthesized using 2 μg of total RNA and *DUOX2* reverse primer with Moloney murine leukemia virus reverse transcriptase (Promega) according to the manufacturer's protocol. The resulting cDNA products were amplified with GoTaq DNA Polymerase (Promega) according to the manufacturer's protocol. The samples were denatured at 95 °C for 5 min followed by 40 cycles of amplification consisting of 1 min 95 °C, 30 s 57 °C and 1 min 72 °C, and a final primer extension of 10 min 72 °C.

PCR primers were designed from *DUOX2* mRNA sequence (NM_014080.4). Four different pairs of primers were used: 16F-19R, 16F-20R, 17F-19R and 17F-20R. The forward primers for exons 16 and 17 were 5-GAGCAGTCCCATCATCATCC-3 (16F) and 5-TGTTTAGTTCTGAAGAGGAACGG-3 (17F), respectively. The reverse primers for exons 19 and 20 were 5-TCATGGTGAAGAATTCGTCCTT-3 (19F) and 5-CATGTCAGCTCCTCCTTGTC-3 (20R), respectively. The expected sizes of the amplified products 16F-19R, 16F-20R, 17F-19R and 17F-20R were 673, 789, 495 and 607 bp, respectively.

The RT-PCR products were purified from the 2% agarose gel by using the Illustra GFX PCR DNA and Gel Band Purification Gel (GE Healthcare), cloned into pGEM-T Easy vector (Promega) and then sequenced with the T7 promoter primer.

2.8. Computer prediction analysis

Searching for potential 5′ ss and 3′ ss sequences in the *DUOX2* gene spanning from intron 17 to intron 18 was accomplished using the NNSplice (http://www.fruitfly.org/seq_tools/splice.html), Fsplice (http://linux1.softberry.com/berry.phtml?topic=fsplice&group=programs&subgroup=gfind), SPL (http://linux1.softberry.com/berry.phtml?topic=spl&group=programs&subgroup=gfind) and SPLM (http://linux1.softberry.com/berry.phtml?topic=splm&group=programs&subgroup=gfind) prediction tools. Scores of the 9-nt sequences corresponding either to authentic and exonic cryptic 5′ ss, were calculated by means of the MaxEntScan program (http://genes.mit.edu/burgelab/maxent/Xmaxentscan_scoreseq.html) by selecting for the analyses the MAXENT, the MDD, the MM, or the WMM. While, scores of the 23-nt sequences, corresponding either to authentic, mutated and cryptic 3′ ss, were calculated by means of the MaxEntScan program (http://genes.mit.edu/burgelab/maxent/Xmaxentscan_scoreseq_acc.html) by selecting for the analyses the MAXENT, the MM, or the WMM.

Finally, the analysis of nucleotide sequences that allows the identification of putative exonic splicing enhancer (ESE) responsive to the human Ser/Arg-rich proteins (SR proteins) (Blencowe, 2000) was performed using the ESEfinder program (http://rulai.cshl.edu/tools/ESE/).

3. Results

3.1. Screening of mutations in the TPO and DUOX2 genes by SSCP and sequence analysis

Promoter and all 17 exons of *TPO* gene and all 33 coding exons of the *DUOX2* gene, along with the flanking intronic sequences, from patient II-1 and healthy controls were screened by SSCP analysis. The analysis of *TPO* PCR products did not show aberrant bands, suggesting the absence of *TPO* gene mutations. Whereas, analysis of *DUOX2* PCR products showed 2 different patterns of migration that were not detected in the healthy controls. Sequence analysis of the samples showing the abnormal SSCP patterns revealed 1 previously identified mutation and 1 novel mutation. The previously reported 3′ ss mutation in intron 17 was a c.2335-1G>C (Muzza et al., 2014) and the novel mutation was a GAGC deletion in exon 24 (c.3264_3267delCAGC) (Fig. 1).

These findings indicate that index patient II-1 is a compound heterozygous for c.2335-1G>C/c.3264_3267delCAGC (Fig. 1). The c.3264_3267delCAGC heterozygous state of index patient II-1 was confirmed by cloning and sequencing of both wild type and mutant alleles (Fig. 1). Sequencing analysis of PCR products of exons 18 and 24 from index patient II-I, his father (I-1), his mother (I-2), and his unaffected sister showed that II-1 inherited 1 copy of the c.2335-

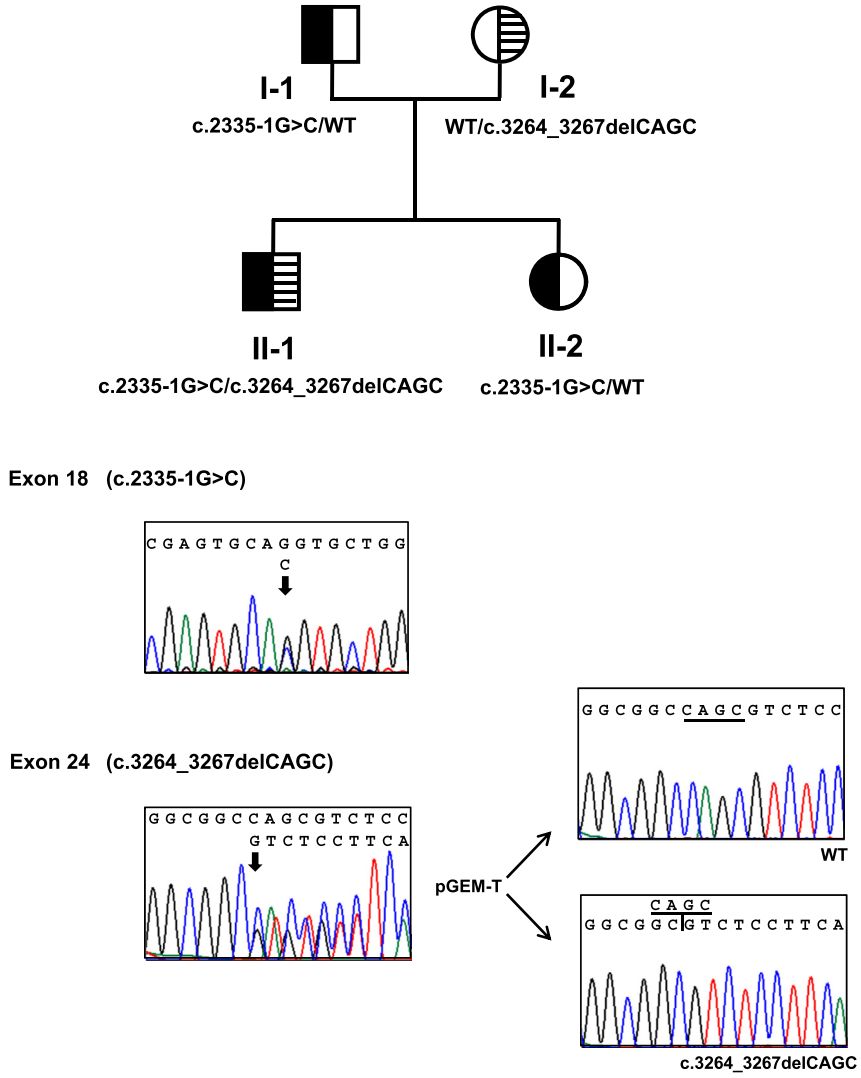

Fig. 1. Mutations in the DUOX2 gene in index patient II-1 and their parents. Partial sequencing chromatograms of genomic DNA from patient II-1 are shown. The pedigree shows the pattern of inheritance of the mutant *DUOX2* alleles. Squares represent males and circles females. Filled symbols denote affected individuals and half-filled symbols, unaffected heterozygote individuals. The solid symbols indicate the c.2335-1G>C mutated allele and the hatched symbols the c.3264_3267delCAGC mutated allele. Sense strand is shown. Arrows denote the position of identified mutations, single chromatogram peaks indicate homozygosity and two overlapping peaks at the same locus, heterozygosity. Partial sequencing chromatograms of wild-type (WT) and mutated (c.3264_3267delCAGC) alleles corresponding to exon 24 from index patient II-1 cloned into pGEM-T Easy vector are shown.

1G>C mutation from his father and 1 copy of the c.3264_3267delCAGC mutation from his mother (Fig. 1). The healthy sister (II-2) was heterozygous for the c.2335-1G>C mutation and did not carry the c.3264_3267delCAGC mutation.

Direct sequencing of *DUOX2* exon 24 revealed the presence of the p.1067S>L polymorphism (Maruo et al., 2008; Muzza et al., 2014) in all members of the family, in homozygous state.

3.2. Minigene analysis

To assess the impact of the c.2335-1G>C ss mutation, minigene constructs were generated and tested in transiently transfected cultured cells by RT-PCR amplification. Wild-type and mutated RT-PCR fragments were cloned in pGEM-T Easy vector and then sequenced with the pSPL3F and pSPL3R vector primer. Fig. 2 illustrates the pattern found in wild type and c.2335-1G>C mutation RT-PCR products. Both amplification reactions displayed three different transcripts: one of them corresponds apparently to the complete included exon 18 (α splicing event), the middle transcript corresponds to the partially included exon 18 (β splicing event) and the smallest transcript is compatible in size with the skipping of exon 18 (γ splicing event). Sequence analysis confirmed the complete inclusion of exon 18 (486 bp), the deletion of 169 nucleotides at the end of exon 18 (317 bp) and their complete exclusion in the wild type transcripts (260 bp) (Fig. 3). The splicing events were similar in c.2335-1G>C minigene compared to the wild type, except that an insertion of the last 14 nucleotides of the intron 17 was identified by sequencing in α (500 bp) and β (331 bp) aberrant splicing events (Fig. 3).

The mutation c.2335-1G>C activated an unusual cryptic donor splice site in intron 17. The putative nucleotide composition is CTCTTTCCCTCCCTCTGCTG/CTG (backslashes indicate the cryptic intron 17 junction site), located at position −14 of the authentic intron 17/exon 18 junction site (Fig. 2).

The internal deletion of exon 18 was anticipated as result to activation of a cryptic site resembling the 5′ ss consensus sequence. The nucleotide composition of cryptic 5′ ss activated is AAG/GTGCGG (backslashes indicate the cryptic exon 18 junction site), 169 nucleotides upstream of the authentic exon 18/intron 18 junction site (Fig. 2).

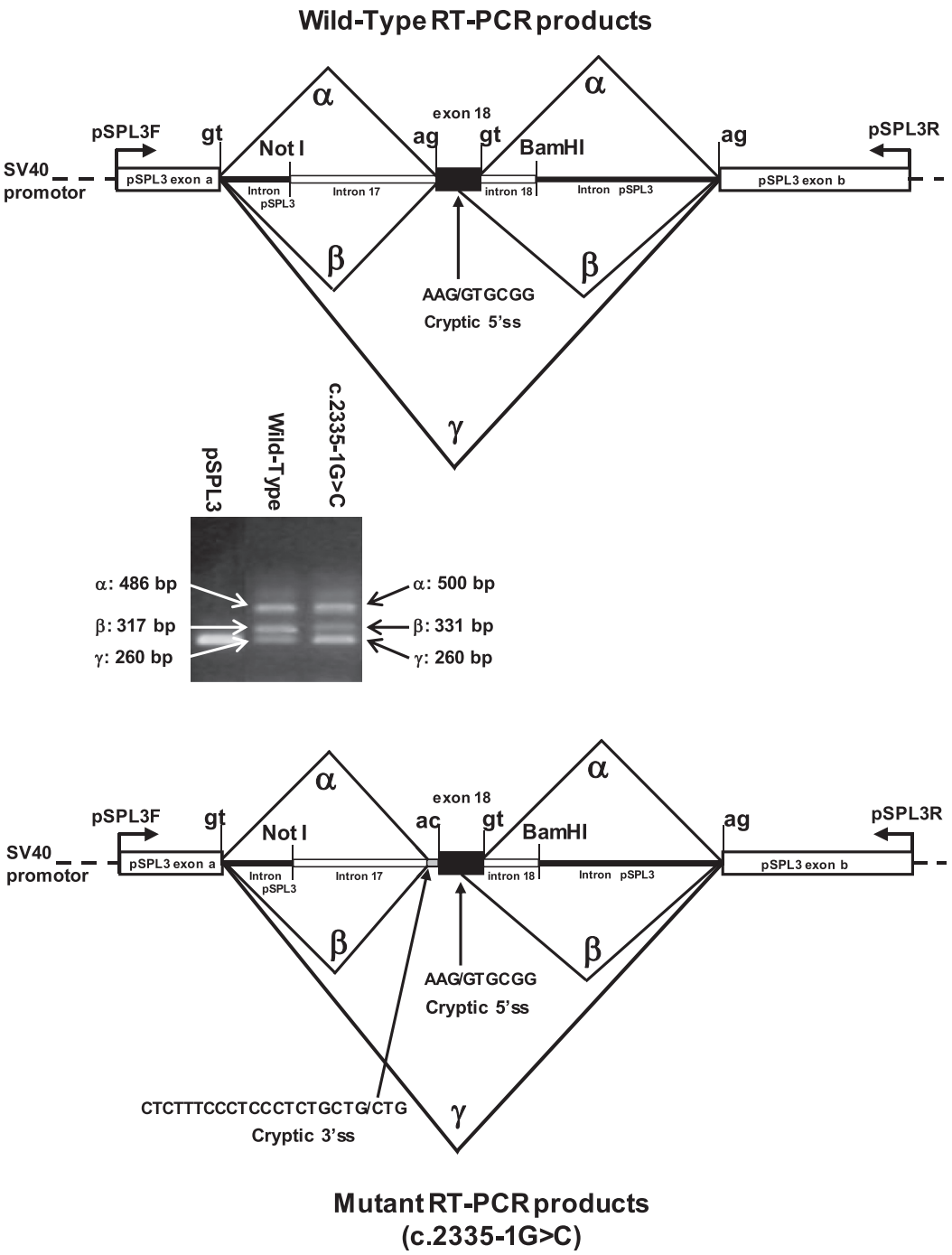

Fig. 2. In vitro expression of the wild-type and c.2335-1G>C mutant minigenes. Schematic representation of the genomic organization of the wild-type and mutant minigenes and their RT-PCR products. The 1519-bp PCR amplified fragment from index patient II-1 was directionally cloned into the NotI and BamHI sites of the exon-trapping pSPL3 vector, which was expressed in HeLa cells. Vector and genomic DNA splice donor (gt) and acceptor (ag) sites are shown. cDNA was synthesized from transcribed mRNA and amplified with pSPL3F and pSPL3R primers complementary to flanking vector sequences. The processing of the wild-type transfected sequences produces RT-PCR products of 486 bp (inclusion exon 18, α splicing event), 317 bp (activation of cryptic 5′ splice site in the exon 18, β splicing event) and 260 bp (skipping of exon 18, γ splicing event). The c.2335-1G>C construct generated also three fragments of 500 pb (α splicing event), 331 pb (β splicing event) and 260 bp (γ splicing event). Mutant α and β splicing events result from splicing at a cryptic site 14 nucleotides 5′ of the correct intron 17 splice acceptor site. RT-PCR products (empty pSPL3 vector, c.2335-1G>C mutant and wild-type) were run on a 2% agarose gel electrophoresis./denotes the cryptic junction site.

3.3. RT-PCR experiment

In order to test whether the two smaller transcripts identified in the expression of wild-type *DUOX2* hybrid minigene are observed in normal thyroid tissue, we performed four different RT-PCRs spanning exons 16–20 (16F-19R, 16F-20R, 17F-19R and 17F-20R products). We detected only bands of the expected size in all products (data not shown).

3.4. 3′ and 5′ splice site prediction analysis

In-silico prediction of the effect of the c.2335-1G>C mutation on splicing showed the expected inactivation of intron 17 acceptor site (Fig. 4a). The location of such substitutions usually has an adverse

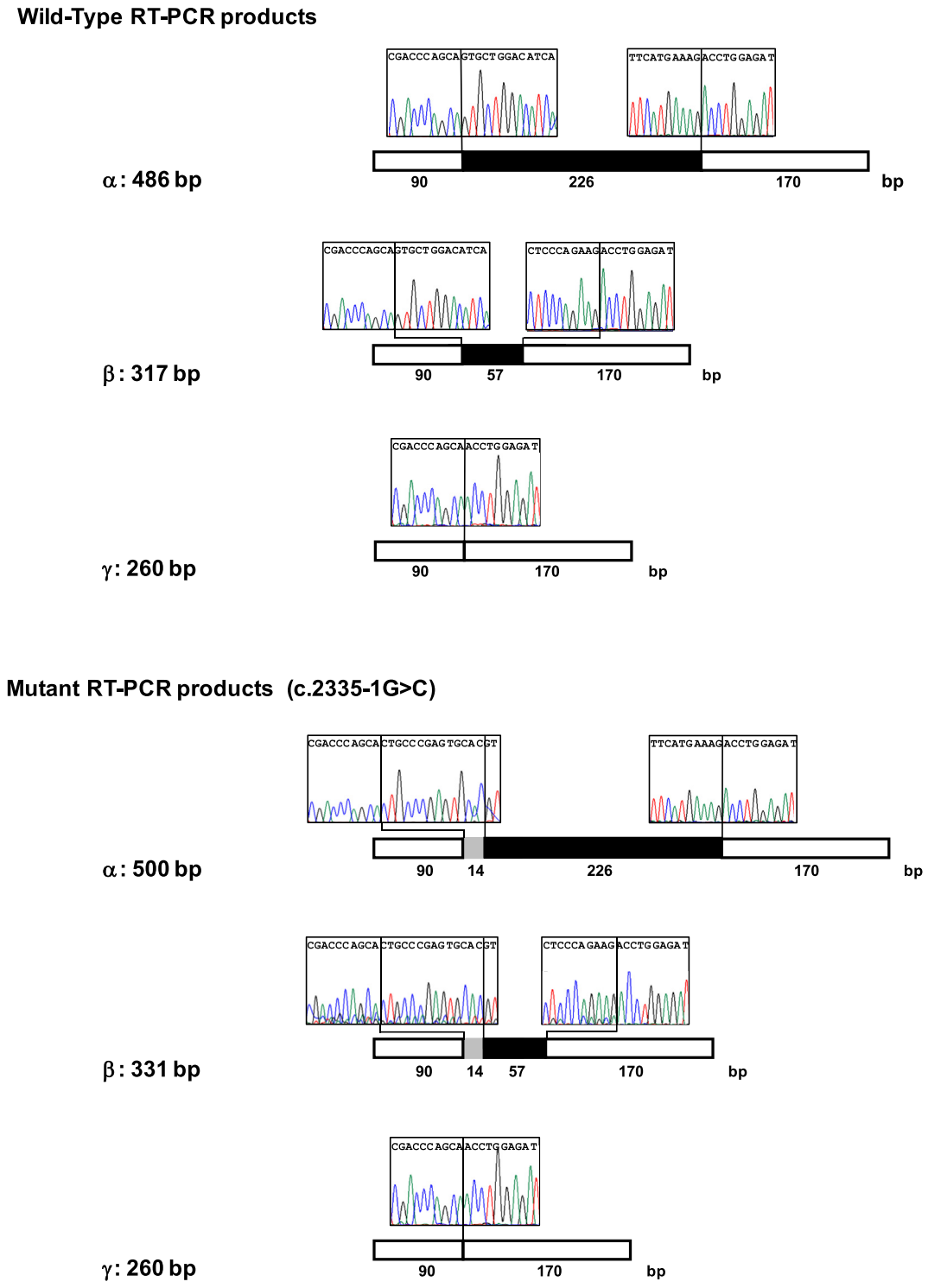

Fig. 3. Direct sequence data from Wild-type and c.2335-1G>C mutant RT-PCR products. The exons from pSPL3 vector (exon a: 90 bp and exon b: 170 bp) and the exon 18 of *DUOX2* (226 bp or 57 bp by activation of cryptic 5′ splice site) are represented by open and dark boxes, respectively. Inclusion of 14 nucleotides in mutant α and β splicing events by activation of a putative intron 17 cryptic site is indicated by gray shaded square. Partial sequencing chromatograms corresponding to α, β and γ splicing events (as described in Fig. 2) are reported above of the respective diagrams.

effect on the recognition of ss by the cellular machinery. NNSplice, FSplice, SPL and SPLM combined prediction program analysis did not identify the mutated 3′ ss as an acceptor site of splicing (Fig. 4a). The strength of cryptic and physiologic sites were also compared by three other methods, the maximum entropy model (MAXENT), the first-order Markov model (MM) and Weight Matrix Model (WMM), that require the prior knowledge of the input sequence to be tested. MAXENT, MM and WMM scores were negatives for the mutated 3′ ss with respect to wild type 3′ ss (Fig. 4a). The putative cryptic 3′ ss identified in intron 17, predicted by minigene analysis, is not identified by NNSplice, FSplice, SPL and SPLM tools, whereas MAXENT, MM and WMM scores were unexpectedly higher for the

a

	Cryptic 3' ss CTCTTTCCCTCCCTCTGCTG/CTG	Wild-type 3' ss CTGCTGCTGCCCGAGTGCAG/GTG	Mutated 3' ss CTGCTGCTGCCCGAGTGCAC/GTG
NNsplice	0.00	0.24	0.00
FSplice	0.00	0.00	0.00
SPL	0.00	0.00	0.00
SPLM	0	10	0
MAXENT	4.57	4.44	-3.62
MM	3.70	2.62	-5.44
WMM	6.59	4.76	-3.31

b

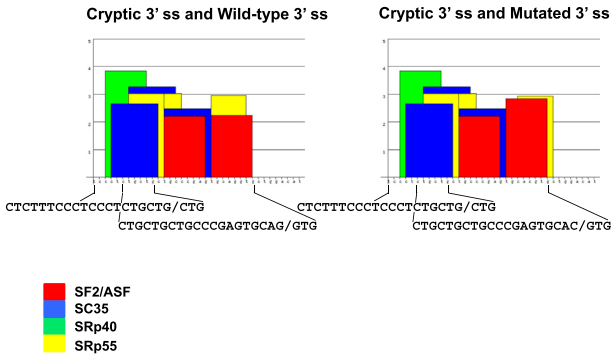

Fig. 4. In Silico analysis of the cryptic, wild-type and mutated 3′ splice sites. a) Individual scores for each 3′ splice site obtained by a panel of acceptor site prediction programs (NNSplice, FSplice, SPL, SPLM, MAXENT, MM and WMM). b) Potential SR binding sites (SF2/ASF, SC35, SRp40 and SRp55) identified by the ESEfinder 3.0 program. The height of each bar represents the motif scores, whereas its width indicates the length of the binding site motifs for SR proteins and its position along the sequence./denotes the cryptic, wild-type and mutated junction sites.

a

	Cryptic 5' ss AAG/GTGCGG	Wild-type 5' ss AAG/GTAGGG
NNsplice	0.70	0.93
Fsplice	9.04	11.28
SPL	0.81	0.94
SPLM	38	62
MAXENT	8.17	8.76
MDD	12.58	13.68
MM	7.51	8.48
WMM	7.41	9.40

b

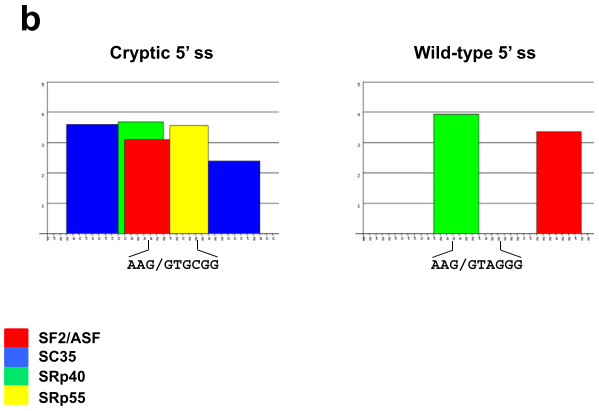

Fig. 5. In Silico analysis of the cryptic and wild-type 5′ splice sites. a) Individual scores for each 5′ splice site obtained by a panel of acceptor site prediction programs (NNSplice, FSplice, SPL, SPLM, MAXENT, MDD, MM and WMM). b) Potential SR binding sites (SF2/ASF, SC35, SRp40 and SRp55) identified by the ESEfinder 3.0 program. The height of each bar represents the motif scores, whereas its width indicates the length of the binding site motifs for SR proteins and its position along the sequence./denotes the cryptic and wild-type junction sites.

cryptic 3′ ss with respect to wild type 3′ ss (Fig. 4a). Interestingly, according to ESEfinder, c.2335-1G>C mutation diminish the score of SF2/ASF protein and changes the position of SRp55 protein that bind to ESE sequence located around the intron 17/exon 18 junction (Fig. 4b).

In order to evaluate the in silico relevance of the cryptic 5′ ss, the potential 5′ ss sequences located in the exon 18 were predicted using the NNSplice, FSplice, SPL and SPLM tools. As shown in Fig. 5a, the exonic cryptic 5′ ss activated, predicted by minigene analysis, was recognized by all programs. MAXENT, MDD (maximum dependence decomposition model), MM and WMM scores were consistently slightly lower for the cryptic 5′ ss with respect to wild type 5′ ss (Fig. 5a). Using the ESEfinder program we observed that the cryptic site has ESE sequences recognizable by SF2/ASF, SRp40 and SRp55 proteins, whereas wild type 5′ ss was recognized by SRp40. (Fig. 5b).

3.5. *DUOX2 proteins prediction analysis*

According to the results obtained by expression of the minigenes, in addition of transcript with complete exon 18 inclusion, the wild type induces proteins with a reading frame change by junction of the partially deleted exon 18 with the exon 19, or the junction of exon 17 (complete exclusion of exon 18) with exon 19. In both cases, two truncated proteins are generated (Fig. 6). Therefore, activation of a cryptic 5′ ss produces a frameshift at amino acid 798 and the skipping of exon 18 results in a frameshift at amino acid 779 (Fig. 6). Both reading frame changes give rise to their respective putative premature stop codons, 8 codons downstream, within exon 19 (Fig. 6). Consequently, the finally encoded protein from the partial deleted exon 18 is predicted to contain 805 residues, including 797 residues of normal *DUOX2* sequences, whereas from the total deleted exon 18 is predicted to contain 786 residues, including 778 residues of normal *DUOX2* sequences (Fig. 6).

Splicing assay with the minigene construct containing c.2335-1G>C mutation provides evidences consistent with the fact of the putative expression of three proteins with a reading frame change, by intron 17 cryptic 3′ ss activation, or by simultaneous activation of intron 17 cryptic 3′ ss and exon 18 cryptic 5′ ss, or by complete exon 18 exclusion (Fig. 7). Therefore, these three mutant forms result in a frameshift at amino acid 779 and in a premature stop, at codon 807 in the first two cases or at codon 787 by complete skipping of exon 18 (Fig. 7).

The c.3264_3267delCAGC mutation results in a frameshift at

Fig. 6. Structural organization of the wild-type DUOX2 proteins generated by intron 17 authentic 3′ splice site activation, exon 18 cryptic 5′ splice site activation and exon 18 skipping. The peroxidase-like and gp91^{phox}/NOX2-like domains, glycosilation sites (NXS/T site), EF-hand calcium motifs, and, FAD and NADPH binding sites, drawn to scale, are shown. The seven alpha helice transmembrane domains are represented by boxes. The partial nucleotide and the deduced amino acid sequences from wild-type are reported below of the respective schematic protein diagrams. The nucleotide sequence is given in the upper line, and the amino acid translation (represented by single-letter code) is given below their respective codons. The nucleotide position in human *DUOX* mRNA is designated according to reference sequences (NCBI, accession number: NM_014080.4). The 'A' of the ATG start codon is denoted as nucleotide +1 being the initiator methionine, the codon 1. The exon 18 cryptic 5′ splice site is boxed. The resulting frameshift by exon 18 cryptic 5′ splice site activation or by exon 18 skipping are underlined. indicates exon/exon boundaries and exon numbering is showed. Splice site, ss; signal peptide, SP.

Wild-Type, intron 17 authentic 3' ss activation

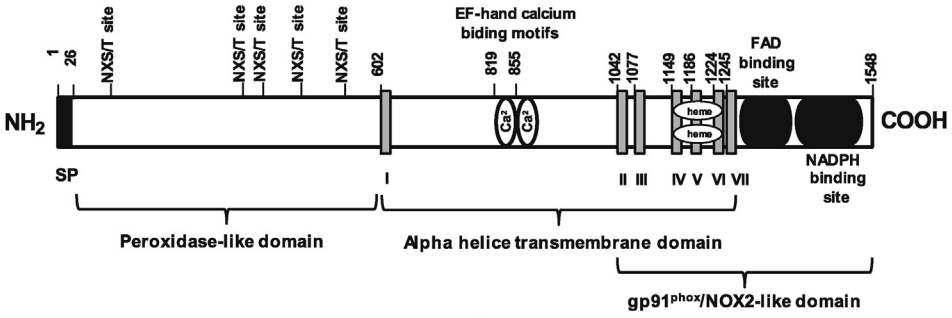


```
2269  aaggctgtgacaaagcagcagcgggaacgcatcctggagatcttcttcagacacctttttt
 757  K  A  V  T  K  Q  Q  R  E  R  I  L  E  I  F  F  R  H  L  F
                17┌18
2329  gctcaggtgctggacatcaaccaggccgacgcagggaccctgcccctggactcctcccag
 777  A  Q  V  L  D  I  N  Q  A  D  A  G  T  L  P  L  D  S  S  Q
2389  aaggtgcgggaggccctgacctgcgagctgagcagggccgagtttgccgagtccctgggc
 797  K  V  R  E  A  L  T  C  E  L  S  R  A  E  F  A  E  S  L  G
2449  ctcaagccccaggacatgtttgtggagtccatgttctctctggctgacaaggatggcaat
 817  L  K  P  Q  D  M  F  V  E  S  M  F  S  L  A  D  K  D  G  N
                                                   18┌19
2509  ggctacctgtccttccgagagttcctggacatcctggtggtcttcatgaaaggctcccca
 837  G  Y  L  S  F  R  E  F  L  D  I  L  V  V  F  M  K  G  S  P
2569  gaggataagtcccgtctaatgtttaccatgtatgacctggatgagaatggcttcctctcc
 857  E  D  K  S  R  L  M  F  T  M  Y  D  L  D  E  N  G  F  L  S
```

Wild-Type, exon 18 cryptic 5' ss activation

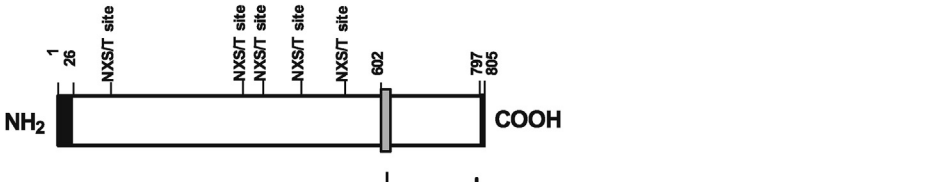


```
2269  aaggctgtgacaaagcagcagcgggaacgcatcctggagatcttcttcagacacctttttt
 757  K  A  V  T  K  Q  Q  R  E  R  I  L  E  I  F  F  R  H  L  F
                17┌18
2329  gctcaggtgctggacatcaaccaggccgacgcagggaccctgcccctggactcctcccag
 777  A  Q  V  L  D  I  N  Q  A  D  A  G  T  L  P  L  D  S  S  Q
                18┌19
2389  aaggctccccagaggataagtcccgtctaatgtttaccatgtatgacctggatgagaatg
 797  K  A  P  Q  R  I  S  P  V  X
```

Wild-Type, exon 18 skipping

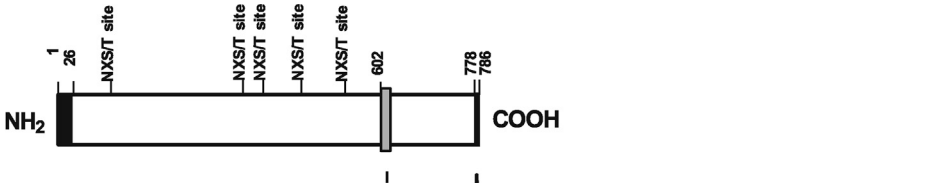


```
2269  aaggctgtgacaaagcagcagcgggaacgcatcctggagatcttcttcagacacctttttt
 757  K  A  V  T  K  Q  Q  R  E  R  I  L  E  I  F  F  R  H  L  F
                17┌19
2329  gctcaggctccccagaggataagtcccgtctaatgtttaccatgtatgacctggatgaga
 777  A  Q  A  P  Q  R  I  S  P  V  X
```

amino acid 1088 with a putative premature stop codon 17 codons downstream, located in the same exon 24 (p.A1088fsX17 or p.A1088fsX1105) (Fig. 8). However, the 1088 alanine did not change (GCC > GCG). Consequently, the finally encoded protein is predicted to contain 1104 residues, including 1088 residues of normal *DUOX2* sequence (Fig. 8).

4. Discussion

Here we describe such a case, which represents a new heterozygous compound c.2335-1G>C/c.3264_3267delCAGC in the *DUOX2* gene. Mutations in the *DUOX2* gene have been conclusively shown to cause CH, a disorder that in some circumstances could be compensated by expression of DUOX1 in the thyroid (Hoste et al., 2010). A patient harbouring *DUOX2* mutations is predicted to have at birth a mild-severe CH with a thyroid gland of normal or enlarged volume and partial or total IOD, depending on the severity of the defect (Fugazzola et al., 2011). Affected individual have clinical and biochemical criteria suggestive of CH associated with IOD: high serum TG and high levels of serum TSH with simultaneous low levels of circulating thyroid hormones (Targovnik et al., 2011). In untreated patients, a complete defect causes a severe phenotype resulting in mental retardation with a goiter. The measurement of TG serum concentrations help to differentiate patients with IOD of those with *IYD* or *TG* mutations. Very low TG concentrations are specific for the diagnosis of *TG* defects (Targovnik et al., 2011), whereas patients with IOD or *IYD* mutations have elevated or very elevated serum TG levels. A significant discharge of thyroidal radioiodine after PDT is consistent with IOD. Unfortunately, PDT from patient II-1 was unavailable. However, the high levels of TG allowed us to orient our study to a defect of IOD and therefore analyze the *TPO* and *DUOX2* genes, major genes involved in the generation of this disorder.

In this study, we used an ex-vivo splicing assay based on a minigene hybrid system and bioinformatics tools to examine the effects at the pre-mRNA level of a ss mutation, c.2335-1G>C, in the *DUOX2* gene (Figs. 2 and 3). Defects in pre-mRNA splicing have been shown as a common disease-causing mechanism in a considerable number of pathophysiological entities, either by altering positions of ss consensus sequences or by affecting intronic or exonic splicing regulatory sequences (Bonnet et al., 2008; Tournier et al., 2008). Most commonly, the consequence of mutations in the natural 5′ and 3′ ss corresponding to higher eukaryotes is skipping of the adjacent exon, followed by activation of donor and acceptor cryptic sequences within adjacent exon or intron sequences, whereas intron retention is very rare (Roca et al., 2003; Buratti et al., 2007). In the literature only three *DUOX2* splice site mutations are reported, c.2335-1G>C (Muzza et al., 2014), also identified in this study, c.2654G>T in exon 19 (Narumi et al., 2011) and c.2655-2A>C (g.IVS19-2A>C) (Varela et al., 2006). Muzza et al., (2014) identified the c.2335-1G>C mutation and performed RT-PCRs (spanning exons 17–19) from RNA extracted from peripheral leukocytes. They detected only bands of the expected size and hypothesize that the mutated spliced allele could be submitted to degradation. The usefulness of splicing reporter minigene assays has been shown to be a good approach to determine the effect of the variants on the splicing process (Bonnet et al., 2008; Tournier et al., 2008). A high level of concordance between data obtained with minigene assays and data from patient's RNA has been shown (Bonnet et al., 2008). Because the blood cells and thyroid tissue from II-1 were unavailable we used hybrid minigen constructs to evaluate c.2335-1G>C mutation. For c.2335-1G>C mutation, minigene and computer-assisted 3′ ss prediction analysis recognized a significant difference between the wild-type and the mutant sequences, suggesting that they might have an impact on the *DUOX2* splicing (Fig. 4). On the other hand, the analysis of mutated minigenes led to the identification of an unusual cryptic donor site in intron 17. Interestingly, the present study shows experimental evidence of activation of a cryptic 5′ ss in both, wild type and mutant pre-mRNAs (Fig. 5). Several studies have suggested that cryptic 5′ ss scores are generally lower than those calculated for the authentic ss (Roca et al., 2003). The local context of the cryptic sites allows the splicing machinery to actively discriminate against their usage and in favor of natural sites (Roca et al., 2003). Here we describe that NNSplice, FSplice, SPL, SPLM, MAXENT, MDD, MM and WMM tools show a slightly lower score for the cryptic 5′ ss than for the authentic 5′ ss (Fig. 5). ESE sequences act as exonic binding sites for SR proteins (SF2/ASF, SC35, SRp40 and SRp55) (Blencowe, 2000). ESE motifs were identified in the vicinity of the ss of constitutive and alternative exons (Wang et al., 2005). In this work we report the identification of ESE binding sites potentially recognizable by SF2/ASF, SRp40 and SRp55 proteins within cryptic 5′ss in exon 18 of the *DUOX2* gene, whereas around of wild type 5′ ss was identified a binding site only for SRp40 protein (Fig. 5). In this context, we hypothesize that the similar score for the cryptic 5′ ss than for the natural 5′ ss and the significant strong presence of ESE binding site for SR proteins within cryptic 5′ ss, are consistent evidence for the activation of the cryptic 5′ ss in the context of wild type and mutant pre-mRNAs. Consequently, the cryptic 5′ ss of exon 18 does not remain silent despite the presence of an authentic active site.

An interesting observation in the present study is the identification of two smaller transcripts from wild-type *DUOX2* hybrid minigene expression, theoretically compatibles with putative truncated proteins of 805 and 786 amino acids, by activation of the exonic cryptic 5′ ss and complete skipped of exon 18, respectively (Fig. 6). However, we observed only a band of the expected size in normal thyroid tissue by RT-PCR. It can be hypothesized that the two smaller spliced transcripts identified in wild-type minigene hybrid system could represent adequate targets, in the thyroid environment, for nonsense-mediated mRNA decay (NMD) pathway, a mechanism that degrades selectively mRNAs containing premature stop codons (Hentze and Kulozik, 1999). This study also showed that the c.2335-1G>C mutation originates two putative truncated proteins of 806 amino acids when the unusual intronic cryptic 3′ ss is activated alone or in combination with activation of the exonic cryptic 5′ ss and 786 amino acids when exon 18 is complete skipped (Fig. 7), whereas the c.3264_3267delCAGC mutation results in a putative truncated protein of 1105 amino acids (Fig. 8). The functional consequence of the frameshift and subsequent premature stop codon, generated by missplicing of *DUOX2* pre-mRNA, could be the complete ability loss to generate thyroid H_2O_2, providing a causal link with the IOD. All premature termination codons in wild-type and mutated proteins eliminate the $gp91^{phox}$/NOX2-like domain, preserving the peroxidase-like domain (Figs. 6–8). It has been demonstrated that isolated human $DUOX2_{1\text{-}599}$ ectodomain displays no peroxidase activity (Meitzler and Ortiz de Montellano, 2011).

From our study, we can draw five conclusions: First, molecular analysis of a patient with hereditary hypothyroidism and normal size thyroid gland reveals a novel heterozygous compound, c.2335-1G>C/c.3264_3267delCAGC in the *DUOX2* gene. Second, functional analysis demonstrated that the wild type and c.2335-1G>C minigenes express three different transcripts: (1) complete inclusion of exon 18, (2) partial inclusion of exon 18 by use of cryptic 5′ splice site located to 169 nucleotides upstream of the wild type exon 18/intron 18 junction and (3) skipping of the entire exon 18. Third, the c.2335-1G>C mutation promotes the activation of a unusual cryptic 3′ ss localized in the intron 17 at 14 nt upstream the wild type intron 17/exon 18 junction, with the resulting insertion of the last 14 nucleotides of the intron 17 in mutant transcripts with complete

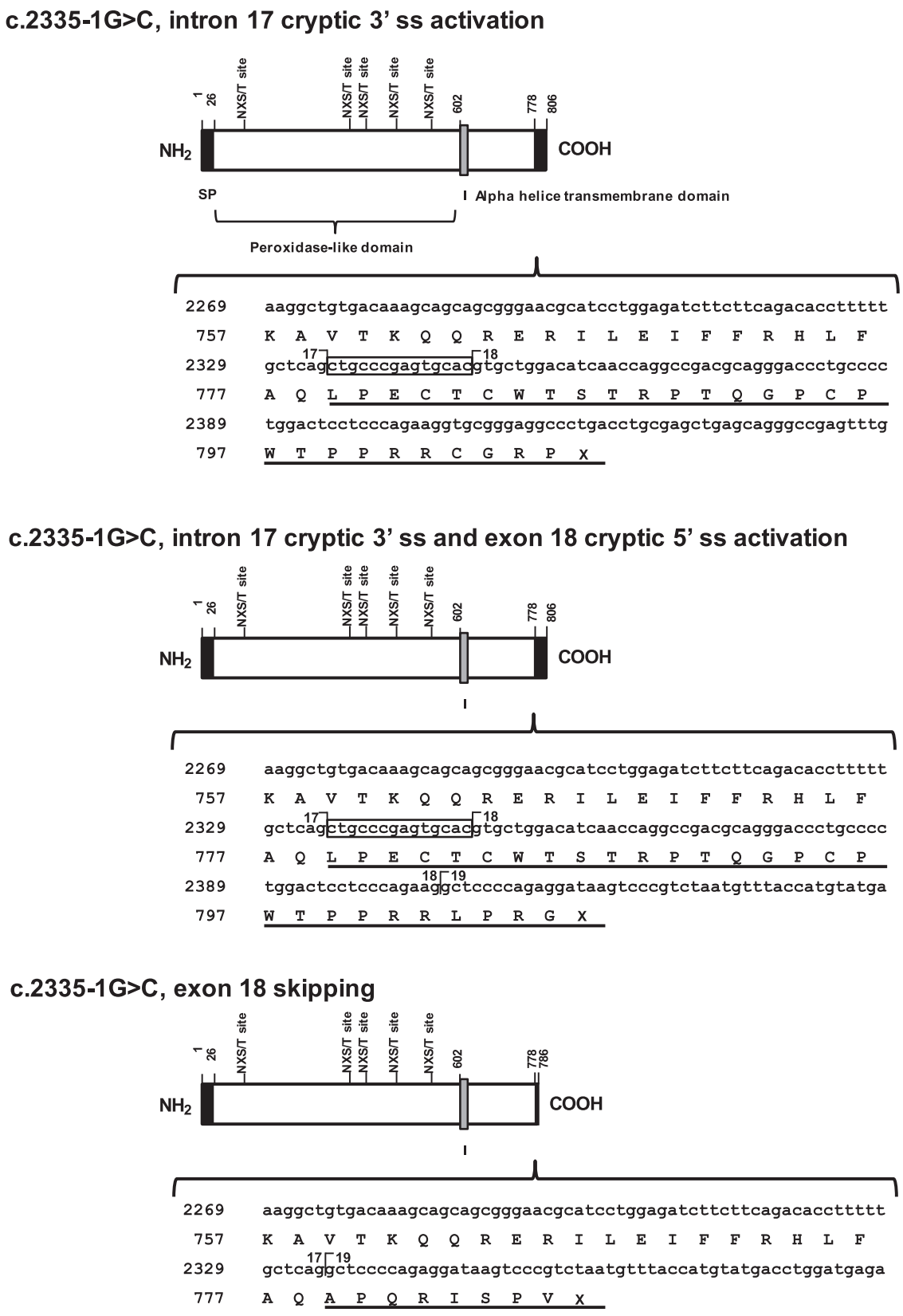

Fig. 7. Structural organization of the putative c.2335-1G>C mutation DUOX2 proteins by intron 17 cryptic 3′ splice site activation, simultaneous activation of intron 17 cryptic 3′ and exon 18 cryptic 5′ splice sites and exon 18 skipping. The peroxidase-like domain and glycosilation sites (NXS/T site), are shown. The first alpha helice transmembrane domain is represented by a box. The partial nucleotide and the deduced amino acid sequences from putative c.2335-1G>C mutants are reported below of the respective schematic protein diagrams. The nucleotide sequence is given in the upper line, and the amino acid translation (represented by single-letter code) is given below their respective codons. The nucleotide position in human *DUOX2* mRNA is designated according to reference sequences (NCBI, accession number: NM_014080.4). The 'A' of the ATG start codon is denoted as nucleotide +1 being the initiator methionine, the codon 1. The last 14 nucleotides of intron 17 which it is included in the transcript by activation of cryptic 3′ splice site, located in intron 17, is boxed. The resulting frameshift by the inclusion of last 14 nucleotides of intron 17 or by exon 18 skipping are underlined. ⌜ indicates exon/exon boundaries and exon numbering is showed. Splice site, ss; signal peptide, SP.

Wild-Type

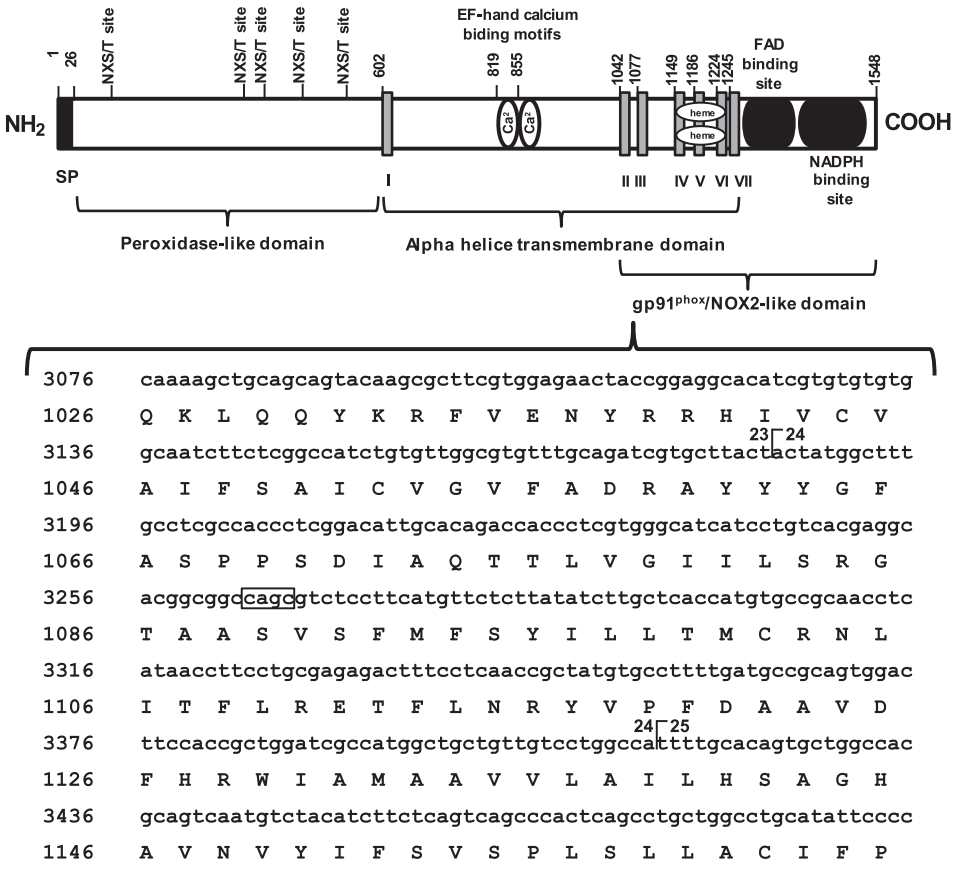

c.3264_3267delCAGC (p.A1088fsX17)

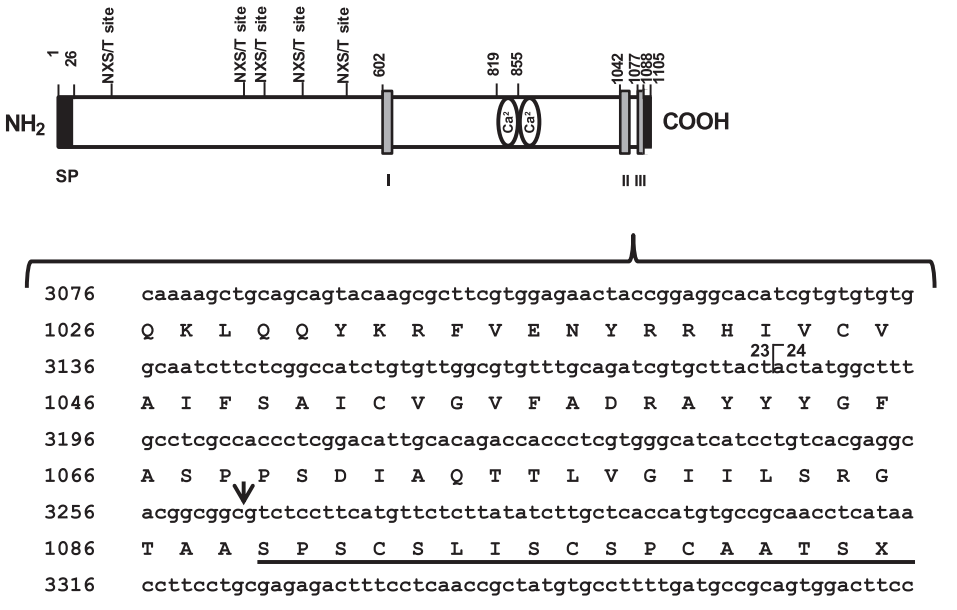

Fig. 8. Structural organization of the wild-type and putative c.3264_3267delCAGC (p.A1088fsX17) DUOX2 proteins. The peroxidase-like and gp91^{phox}/NOX2-like domains, glycosilation sites (NXS/T site), EF-hand calcium motifs and FAD and NADPH binding sites, drawn to scale, are shown. The seven alpha helice transmembrane domains are represented by boxes. The partial nucleotide and the deduced amino acid sequences from wild-type and putative c.3264_3267delCAGC mutants are reported below of the respective schematic protein diagrams. The nucleotide sequence is given in the upper line, and the amino acid translation (represented by single-letter code) is given below their respective codons. The nucleotide position in human *DUOX2* mRNA is designated according to reference sequences (GenBank, accession number: NM_014080.4). The 'A' of the ATG start codon is denoted as nucleotide +1 being the initiator methionine, the codon 1. The c.3264_3267delCAGC mutation is boxed in the wild-type sequence. The arrow denotes the positions of the c.3264_3267delCAGC mutation in the mutant sequences and the resulting frameshift is underlined. ⌜ indicates exon/exon boundaries and exon numbering is showed. Signal peptide, SP.

and partial inclusion of exon 18. Fourth, these results suggest the coexistence in our patient of four putative truncated proteins of 786, 805, 806 and 1105 amino acids, with conservation of peroxidase-like domain and loss of gp91^{phox}/NOX2-like domain. Finally, the present study provides new insights on the role of the *DUOX2* inactivating mutations in the generation of dyshormonogenesis, and on the particular effect of c.2335-1G>C mutation on the mechanism of *DUOX2* splicing.

Disclosure summary

The authors have nothing to disclose.

Acknowledgments

F.S. Belforte and C.E. Citterio are research fellows of the Consejo Nacional de Investigaciones Científicas y Técnicas (CONICET).

C.M. Rivolta and H.M. Targovnik are established investigators of the CONICET.

This study was supported by grants from the Universidad de Buenos Aires (20020100100594/2011 to CMR), CONICET (PIP 2012/112-201101-00091 to HMT) and ANPCyT-FONCyT (PICT 2010/05-1130 to CMR, PICT 2012/05-1090 to HMT).

References

Abe, K., Narumi, S., Suwanai, A.S., Hamajima, T., Hasegawa, T., 2015. Pseudodominant inheritance in a family with nonautoimmune hypothyroidism due to biallelic *DUOX2* mutations. Clin. Endocrinol. Oxf. http://dx.doi.org/10.1111/cen.12622.

Bizhanova, A., Kopp, P., 2010. Genetics and phenomics of Pendred syndrome. Mol. Cell. Endocrinol. 322, 83–90.

Blencowe, B.J., 2000. Exonic splicing enhancers: mechanism of action, diversity and role in human genetic diseases. Trends Biochem. Sci. 25, 106–110.

Bonnet, C., Krieger, S., Vezain, M., Rousselin, A., Tournier, I., Martins, A., et al., 2008. Screening *BRCA1* and *BRCA2* unclassified variants for splicing mutations using reverse transcription PCR on patient RNA and an ex vivo assay based on a splicing reporter minigene. J. Med. Genet. 45, 438–446.

Buratti, E., Chivers, M., Královičová, J., Romano, M., Baralle, M., Krainer, A.R., et al., 2007. Aberrant 5′ splice sites in human disease genes: mutation pattern, nucleotide structure and comparison of computational tools that predict their utilization. Nucleic Acids Res. 35, 4250–4263.

Cangul, H., Aycan, Z., Kendall, M., Bas, V.N., Saglam, Y., Barrett, T.G., et al., 2014. A truncating *DUOX2* mutation (R434X) causes severe congenital hypothyroidism. J. Pediatr. Endocr. Met. 27, 323–327.

Cavarzere, P., Castanet, M., Polak, M., Raux-Demay, M.C., Cabrol, S., Carel, J.C., et al., 2008. Clinical description of infants with congenital hypothyroidism and iodide organification defects. Horm. Res. 70, 240–248.

Chai, J., Yang, X.L., Guo, M.Z., Liu, L., Liu, S.G., Yan, S.L., et al., 2015. *DUOX2* mutations in children with congenital hypothyroidism. Chin. J. Contemp. Pediatr. 17, 40–44.

De Deken, X., Wang, D., Many, M.C., Costagliola, S., Libert, F., Vassart, G., et al., 2000. Cloning of two human thyroid cDNAs encoding new members of the NADPH oxidase family. J. Biol. Chem. 275, 23227–23233.

De Marco, G., Agretti, P., Montanelli, L., Di Cosmo, C., Bagattini, B., De Servi, M., et al., 2011. Identification and functional analysis of novel dual oxidase 2 (*DUOX2*) mutations in children with congenital or subclinical hypothyroidism. J. Clin. Endocrinol. Metab. 96, E1335–E1339.

Di Candia, S., Zamproni, I., Cortinovis, F., Passoni, A., Vigone, M.C., Fugazzola, L., Persani, L., Weber, G., 2006. Congenital hypothyroidism and partial iodide organification defects: two mutations in *DUOX2* gene. Horm. Res. 65 (Suppl. 4), 38.

Dupuy, C., Ohayon, R., Valent, A., Noël-Hudson, M.S., Dème, D., Virion, A., 1999. Purification of a novel flavoprotein involved in the thyroid NADPH oxidase. Cloning of the porcine and human cDNAs. J. Biol. Chem. 274, 37265–37269.

Fugazzola, L., Muzza, M., Weber, G., Beck-Peccoz, P., Persani, L., 2011. *DUOXS* defects: genotype-phenotype correlations. Ann. Endocrinol. Paris. 72, 82–86.

Grasberger, H., De Deken, X., Miot, F., Pohlenz, J., Refetoff, S., 2007. Missense mutations of dual oxidase 2 (*DUOX2*) implicated in congenital hypothyroidism have impaired trafficking in cells reconstituted with *DUOX2* maturation factor. Mol. Endocrinol. 21, 1408–1421.

Grasberger, H., 2010. Defects of thyroidal hydrogen peroxide generation in congenital hypothyroidism. Mol. Cell. Endocrinol. 322, 99–106.

Grasberger, H., De Deken, X., Mayo, O.B., Raad, H., Weiss, M., Liao, X.-H., et al., 2012. Mice deficient in dual oxidase maturation factors are severely hypothyroid. Mol. Endocrinol. 26, 481–492.

Grasberger, H., Refetoff, S., 2011. Genetic causes of congenital hypothyroidism due to dyshormonogenesis. Curr. Opin. Pediatr. 23, 421–428.

Hentze, M.W., Kulozik, A.E., 1999. A perfect message: RNA surveillance and nonsense-mediated decay. Cell 96, 307–310.

Hoste, C., Rigutto, S., Van Vliet, G., Miot, F., De Deken, X., 2010. Compound heterozygosity for a novel hemizygous missense mutation and a partial deletion affecting the catalytic core of the H2O2-generating enzyme *DUOX2* associated with transient congenital hypothyroidism. Hum. Mutat. 31, E1304–E1319.

Hulur, I., Hermanns, P., Nestoris, C., Heger, S., Refetoff, S., Pohlenz, J., et al., 2011. A single copy of the recently identified dual oxidase maturation factor (*DUOXA*) *1* gene produces only mild transient hypothyroidism in a patient with a novel biallelic *DUOXA2* mutation and monoallelic *DUOXA1* deletion. J. Clin. Endocrinol. Metab. 96, E841–E845.

Jin, H.Y., Heo, S.H., Kim, Y.M., Kim, G.H., Choi, J.H., Lee, B.H., et al., 2014. High frequency of *DUOX2* mutations in transient or permanent congenital hypothyroidism with eutopic thyroid glands. Horm. Res. Paediatr. 82, 252–260.

Kasahara, T., Narumi, S., Okasora, K., Takaya, R., Tamai, H., Hasegawa, T., 2013. Delayed onset congenital hypothyroidism in a patient with *DUOX2* mutations and maternal iodine excess. Am. J. Med. Genet. A 161A, 214–217.

Liu, S., Liu, L., Niu, X., Lu, D., Xia, H., Yan, S., 2015. A novel missense mutation (I26M) in *DUOXA2* causing congenital goiter hypothyroidism impairs NADPH oxidase activity but not protein expression. J. Clin. Endocrinol. Metab. 100, 1225–1229.

Lü, Z.P., Li, G.H., Li, W.J., Liu, S.G., 2011. *DUOX2* gene mutation in patients with congenital goiter with hypothyroidism. Zhonghua Er Ke Za Zhi 49, 943–946.

Maruo, Y., Takahashi, H., Soeda, I., Nishikura, N., Matsui, K., Ota, Y., et al., 2008. Transient congenital hypothyroidism caused by biallelic mutations of the dual oxidase 2 gene in Japanese patients detected by a neonatal screening program. J. Clin. Endocrinol. Metab. 93, 4261–4267.

Meitzler, J.L., Ortiz de Montellano, P.R., 2011. Structural stability and heme binding potential of the truncated human dual oxidase 2 (*DUOX2*) peroxidase domain. Arch. Biochem. Biophys. 512, 197–203.

Morand, S., Dos Santos, O.F., Ohayon, R., Kaniewski, J., Noel-Hudson, M.-S., Virion, A., et al., 2003. Identification of a truncated dual oxidase 2 (*DUOX2*) messenger ribonucleic acid (mRNA) in two rat thyroid cell lines. Insulin and forskolin regulation of *DUOX2* mRNA levels in FRTL-5 cells and porcine thyrocytes. Endocrinology 144, 567–574.

Morand, S., Agnandji, D., Noel-Hudson, M.S., Nicolas, V., Buisson, S., Macon-Lemaitre, L., et al., 2004. Targeting of the dual oxidase 2 N-terminal region to the plasma membrane. J. Biol. Chem. 279, 30244–30251.

Moreno, J.C., Bikker, H., Kempers, M.J.E., van Trotsenburg, A.S.P., Baas, F., de Vijlder, J.J.M., et al., 2002. Inactivating mutations in the gene for thyroid oxidase 2 (*THOX2*) and congenital hypothyroidism. N. Engl. J. Med. 347, 95–102.

Moreno, J.C., Visser, T.J., 2010. Genetics and phenomics of hypothyroidism and goiter due to iodotyrosine deiodinase (*DEHAL1*) gene mutations. Mol. Cell. Endocrinol. 322, 91–98.

Muzza, M., Rabbiosi, S., Vigone, M.C., Zamproni, I., Cirello, V., Maffini, M.A., et al., 2014. The clinical and molecular characterization of patients with dyshormonogenic congenital hypothyroidism reveals specific diagnostic clues for *DUOX2* defects. J. Clin. Endocrinol. Metab. 99, E544–E553.

Narumi, S., Muroya, K., Asakura, Y., Aachi, M., Hasegawa, T., 2011. Molecular basis of thyroid dyshormonogenesis: genetic screening in population-based Japanese patients. J. Clin. Endocrinol. Metab. 96, E1838–E1842.

Ohye, H., Fukata, S., Hishinuma, A., Kudo, T., Nishihara, E., Ito, M., et al., 2008. A novel homozygous missense mutation of the dual oxidase 2 (*DUOX2*) gene in an adult patient with large goiter. Thyroid 18, 561–566.

Oyhe, H., Sugawara, M., 2010. Dual oxidase, hydrogen peroxide and thyroid diseases. Exp. Biol. Med. 235, 424–433.

Pfarr, N., Korsch, E., Kaspers, S., Herbst, A., Stach, A., Zimmer, C., et al., 2006. Congenital hypothyroidism caused by new mutations in the thyroid oxidase 2 (*THOX2*) gene. Clin. Endocrinol. Oxf. 65, 810–815.

Ris-Stalpers, C., Bikker, H., 2010. Genetics and phenomics of hypothyroidism and goiter due to *TPO* mutations. Mol. Cell. Endocrinol. 322, 38–43.

Rivolta, C.M., Esperante, S.A., Gruñeiro-Papendieck, L., Chiesa, A., Moya, C.M., Domené, S., et al., 2003. Five novel inactivating mutations in the human thyroid peroxidase gene responsible for congenital goiter and iodide organification defect. Hum. Mutat. 22, 259.

Roca, X., Sachidanandam, R., Krainer, A.R., 2003. Intrinsic differences between authentic and cryptic 5′ splice sites. Nucleic Acids Res. 31, 6321–6333.

Satoh, M., Aso, K., Ogikubo, S., Yoshizawa-Ogasawara, A., Saji, T., 2015. Hypothyroidism caused by the combination of two heterozygous mutations: one in the *TSH* receptor gene the other in the *DUOX2* gene. J. Pediatr. Endocrinol. Metab. 28, 657–661.

Schoenmakers, N., Cangul, H., Nicholas, A.K., Schoenmakers, E., Lyons, G., Dattani, M., et al., 2013. A comprehensive next generation sequencing-based strategy for genetic diagnosis in congenital hypothyroidism. Endocr. Abstr. 33. OC2.9.

Spitzweg, C., Morris, J.C., 2010. Genetics and phenomics of hypothyroidism and goiter due to *NIS* mutations. Mol. Cell. Endocrinol. 322, 56–63.

Targovnik, H.M., Esperante, S.A., Rivolta, C.M., 2010. Genetics and phenomics of hypothyroidism and goiter due to thyroglobulin mutations. Mol. Cell. Endocrinol. 322, 44–55.

Targovnik, H.M., Citterio, C.E., Rivolta, C.M., 2011. *Thyroglobulin* gene mutations in congenital hypothyroidism. Horm. Res. Paediatr. 75, 311–321.

Tonacchera, M., De Marco, G., Agretti, P., Montanelli, L., Di Cosmo, C., Freitas Ferreira, A.C., et al., 2009. Identification and functional studies of two new dual-oxidase 2 (*DUOX2*) mutations in a child with congenital hypothyroidism and a

eutopic normal-size thyroid gland. J. Clin. Endocrinol. Metab. 94, 4309–4314.
Tournier, I., Vezain, M., Martins, A., Charbonnier, F., Baert-Desurmont, S., Olschwang, S., et al., 2008. A large fraction of unclassified variants of the mismatch repair genes *MLH1* and *MSH2* is associated with splicing defects. Hum. Mutat. 29, 1412–1424.
Varela, V., Rivolta, C.M., Esperante, S.A., Gruñeiro-Papendieck, L., Chiesa, A., Targovnik, H.M., 2006. Three mutations (p.Q36H, p.G418fsX482, and g.IVS19-2A_C) in the dual oxidase 2 gene responsible for congenital goiter and iodide organification defect. Clin. Chem. 52, 182–191.
Vigone, M.C., Fugazzola, L., Zamproni, I., Passoni, A., Di Candia, S., Chiumello, G., et al., 2005. Persistent mild hypothyroidism associated with novel sequence variants of the *DUOX2* gene in two siblings. Hum. Mutat. 26, 395.
Wang, F., Lu, K., Yang, Z., Zhang, S., Lu, W., Zhang, L., et al., 2014. Genotypes and phenotypes of congenital goitre and hypothyroidism caused by mutations in dual oxidase 2 genes. Clin. Endocrinol. Oxf. 81, 452–457.
Wang, J., Smith, P.J., Krainer, A.R., Zhang, M.Q., 2005. Distribution of SR protein exonic splicing enhancer motifs in human protein-coding genes. Nucleic Acids Res. 33, 5053–5062.
Yi, R.-H., Zhu, W.-B., Yang, L.-Y., Lan, L., Chen, Y., Zhou, J.-F., et al., 2013. A novel dual oxidase maturation factor 2 gene mutation for congenital hypothyroidism. Int. J. Mol. Med. 31, 467–470.
Yoshizawa-Ogasawara, A., Ogikubo, S., Satoh, M., Narumi, S., Hasegawa, T., 2013. Congenital hypothyroidism caused by a novel mutation of the dual oxidase 2 (*DUOX2*) gene. J. Pediatr. Endocrinol. Metab. 26, 45–52.
Zamproni, I., Grasberger, H., Cortinovis, F., Vigone, M.C., Chiumello, G., Mora, S., et al., 2008. Biallelic inactivation of the *dual oxidase maturation factor 2 (DUOXA2)* gene as a novel cause of congenital hypothyroidism. J. Clin. Endocrinol. Metab. 93, 605–610.